

Metal-Modified Mesoporous Silicate (MCM-41) Material: Preparation, Characterization and Applications as an Adsorbent

Alejandra S. Diez,^a Mariana Alvarez^{*,a} and Maria A. Volpe^b

^aINQUISUR-CONICET, Departamento de Química, Universidad Nacional del Sur,
B8000CPB Bahía Blanca, Argentina

^bPlanta Piloto de Ingeniería Química, B8000FWB Bahía Blanca, Argentina

Mesoporous silicate (MCM-41) materials, modified with Cu^{II}, Fe^{III} or Al^{III} were prepared by a hydrothermal method and were characterized by nitrogen adsorption at 77 K, X-ray powder diffraction (XRD), transmission electron microscopy (TEM), high-resolution transmission electron microscopy (HRTEM), temperature programmed reduction (TPR), adsorption of pyridine as monitored by Fourier transform infrared spectroscopy (FTIR) and *n*-butylamine titration. The degree of ordering of the mesoporous material was decreased by the presence of Cu, Fe, or Al. The added Fe or Cu gave rise to new acidic and oxidation-reduction sites, while Al resulted in new acidic sites. The hydrothermal stabilities of selected samples were studied as a function of temperature and pH. All the samples were stable in acidic and neutral media at temperatures from 303 to 363 K. Adsorption of phenol on MCM-41 at 303 K was strongly influenced by the pH and by the modification with Cu, Fe, or Al. Phenol adsorption was particularly strong at the Al-modified material at pH 3, apparently due to the acidic character of phenol.

Keywords: MCM-41, metal modification, aqueous stability, phenol adsorption

Introduction

MCM-41 is a hexagonal ordered mesoporous silicate, member of the M41S family. It presents large surface area in the 600-1000 m² g⁻¹ range, high pore volume and uniform distribution of pore size (0.5-8 nm). The long-range space group is *P6mm* and its porous walls are relatively thin, with a width of 0.6-1.2 nm.¹ All these properties allow the employment of M41S materials in several applications such as removal of heavy metal ions,²⁻⁶ desulfurization process⁷ and drug delivery.⁸ Mainly, the adsorption of organic pollutants, as phenolic compounds from waste water should be highlighted.⁹⁻¹³ For this application, as prepared, calcined and MCM-41 functionalized with different grafted groups have been studied,^{10,12,14,15} and the latter systems is the key point for the phenol adsorptive properties of MCM-41. Calcined MCM-41 has a relatively low capacity for phenol adsorption, but a remarkable capacity adsorption of phenol derivatives, as hydroquinone, due to its hydrophilic nature. In the same way, this material has been employed as an adsorbent in the clarification of red wine.^{16,17} On the other

hand non-calcined and functionalized MCM-41 show notable properties for phenol adsorption.

The isomorphous replacement of Si in pure siliceous materials with metals strongly modifies MCM-41 properties. The replacement leads to modifications of the pore diameter and volumes, specific surface area and crystallographic parameters.¹⁸⁻²⁰ Besides, the surface chemistry of silanol is also strongly modified, arising new acidic or basic properties, and also creating new redox sites. On the other hand the incorporation of extra-framework species, such as metal oxides particles, is another way to modify MCM-41, which large surface area allows the incorporation of high loadings of heterospecies. All the above mentioned modifications give rise to new materials that could be envisaged for the employment in the removal of pollutants from water.

The objective of the present work was to synthesize MCM-41 containing Cu, Fe or Al for varying the physicochemical properties of the pure siliceous form. In this way, the following samples were prepared: Cu-MCM-41, Fe-MCM-41, Al-MCM-41 and Fe-Al-MCM-41.

The redox properties of the different samples were studied by temperature programmed reduction (TPR), while the morphological aspects were analyzed by means

*e-mail: alvarezm@criba.edu.ar

of transmission electron microscopy (TEM) and nitrogen sorption measurements (isotherms at 77 K). The acidic properties of the materials were studied by potentiometric titrations with *n*-butylamine and Fourier transform infrared spectroscopy (FTIR) of adsorbed pyridine.

Due to the fact that many of the possible applications of the MCM-41 materials would be performed in aqueous media, a study of the hydrothermal stability of the samples at different pH and temperatures is also carried out.

Finally, a full physicochemical description of the samples, carried out in the context of their applications for removing organic pollutants in aqueous media is performed.

Experimental

Synthesis

The samples were prepared by hydrothermal synthesis following the procedures described by Bore *et al.*,²¹ employing cetyl trimethyl ammonium bromide (CTAB) as surfactant and sodium silicate as silica source. The molar ratio of the precursor solution was 3.4SiO₂:1CTAB:286H₂O. MCM-41 samples containing iron, aluminium or copper were obtained by adding the corresponding nitrates (99%, Merck) to the precursor solution. The Si/Me (Me = Fe, Al, Cu) ratios were 15 or 30. An aluminium/iron mixed sample was also prepared with a Si/Me molar ratio of 60 for each metal. For all the cases, the pH of the final mixture was adjusted to 10 with a 1 mol L⁻¹ HNO₃ solution and kept in a water bath for 8 h at 353 K, in a Teflon[®] bottle in static conditions.

All the samples were washed with distilled water, dried and calcined at 773 K for 12 h at 10 °C min⁻¹.

Samples were named as MeM30 and MeM15, where Me indicates the corresponding metal used during the synthesis procedure and the number refers to the Si/Me molar ratio.

Sample characterization

The metal content was determined by absorption atomic spectroscopy (AAS). The specific surface area of the samples was calculated following the Brunauer-Emmett-Teller (BET) method. N₂ isotherms at 77 K were obtained employing a Nova 1200e Quantachrome equipment. The pore diameter was determined by Barrett-Joyner-Halenda (BJH) method. The relative pressure range employed was 0-1.0 (P/P₀). Samples were pre-treated by an evacuation at 393 K for 20 h before measuring the corresponding isotherm. The samples were characterized by X-ray powder diffraction (XRD). The patterns of the samples were recorded on two different equipments:

Philips PW1710 BASED and Panalytical, Empirean Model. The former one operating at 45 kV and 30 mA fitted with a graphite monochromator in order to get CuK α 1 radiation (15.406 nm); the angle step and counting time were 0.035 (2 θ) and 1 s, respectively. The other equipment was operated at low angles using a Xe detector with curve graphite monochromator and at high angles a Pixcel 3D detector with Ni filter. The angle step and counting time were 0.02 (2 θ) and 2 s, respectively. Transmission electron microscopy (TEM) images were taken in a JEOL 100X2 apparatus. A high-resolution transmission electron microscopy (HRTEM) characterization was carried out over selected samples, in a Philips CM200 UT microscope, operating at 200 kV at room temperature. The samples were dispersed in an ultrasound and placed on an amorphous carbon film.

A temperature programmed reduction (TPR) study was carried out in a home-made apparatus. Samples were previously calcined at 773 K in chromatographic air and purged in N₂. Afterwards, the samples were cooled down to 333-353 K, and the gas was switched to the reactive mixture (H₂/Ar, 10%) with a flow rate of 18 cm³ min⁻¹. The hydrogen uptakes were measured with a thermal conductivity detector (TCD), while the temperature was linearly increased at a rate of 8 °C min⁻¹, up to 773 K.

Fourier transform infrared (FTIR) spectra were recorded in the 4000-400 cm⁻¹ region in a Nicolet Nexus FTIR apparatus. Solids were diluted with KBr (1%).

UV-Vis spectra were recorded on a Cecil 2021 spectrometer. Samples were dispersed in KBr disks (1%) and the spectra were collected in the range of 200-800 nm.

Total acidity of the samples was measured using a potentiometric method of titration with *n*-butylamine²² (0.1 mol L⁻¹, in acetonitrile) which was added to a suspension of 0.10 g of the mesoporous sample in 90 mL employing acetonitrile as the solvent. This system was kept under steady stirring for 3 h at 303 K. The suspension was then titrated by measuring the electrode potential (mV) 2 min after adding base-solution volumes of 0.05 mL each time. The measurements were carried out with an Adwa AD1040 digital pH/mV meter. The electrode potential measured after adding the first volume of titration agent and following 3 h, was considered to be a measurement of the acid strength. Besides, the total number of acid sites was estimated from the total amount of base added to reach the plateau in the potential *vs.* volume curve, and the acid site density was calculated considering the apparent surface area value of the corresponding sample.

In addition, the acidic properties of the samples were studied by FTIR of previously adsorbed pyridine, using an FTIR spectrometer Nicolet Magna-550 with a DTGS KBr

detector and a vacuum cell with CaF_2 window attached to the vacuum apparatus. The probe molecule was put in contact with the sample at 423 K for 20 min with a partial pressure of 3 Torr of pyridine, followed by 20 min evacuation at 423 K and 523 K. The nature of the acid sites (Lewis or Brönsted) was determined from the frequency of the bands of adsorbed pyridine, following previous reports. The concentration of Lewis sites was calculated taking into account the corresponding extinction coefficients.²³

Aqueous stability study of Al-MCM-41 and Fe-MCM-41

The stability in water of samples with a Si/Me ratio of 30 was studied. Approximately 100 mg of the calcined solid were introduced in 100 mL of distilled water at 303, 333 or 363 K and stirred for 6 h. The influence of pH on the stability of the sample was also examined in a similar manner, keeping the temperature at 303, 333 or 363 K, and varying the pH by the addition of acetic acid or ammonia to reach pH values of 3, 6 or 10 respectively. After performing the treatment, the material was washed, filtered and dried at 393 K for 2 h. The samples were studied by XRD, taking the intensity of the main diffraction peak, corresponding to the (100) plane of MCM-41 as a measurement of the mesoporous structure stability. The a_0 parameter was also measured for fresh and water treated samples.

Phenol adsorption

Approximately 100 mg of adsorbent, 100 mL of distilled water and 50 mL of a 60 mg L⁻¹ aqueous solution of phenol (PhOH, Merck) were kept in contact at 303 K for 24 h, in a cylindrical Pyrex[®] vessel. The experiments were carried out at different pH values by employing solutions of ammonium hydroxide (NH_4OH) or acetic acid (CH_3COOH) to reach the desired pH. Afterwards, the adsorbent was filtered and the PhOH concentration in the residual solution was measured by ultraviolet (UV) spectrometry using a Cecil 2021 spectrophotometer, at a wavelength of 287 nm.

Results and Discussion

Samples preparation and characterization

The XRD profiles of the samples show a typical pattern of the hexagonal mesoporous structure (Figure 1). An intense peak at low 2θ angle is detected, due to the diffraction of (100) plane of MCM-41. In addition, other minor peaks attributable to (110), (210) and (200) reflections planes are observed. Comparing the profiles of pure MCM-41 with the corresponding to the modified samples, the main difference is a decrease of the peaks intensity originated by a loss of the mesoporous order due to the presence of metal species. Such distortion was already reported for some of us in a previous work regarding Cu/MCM-48²⁴ and it is undoubtedly related to a high interaction of Me species with MCM-41 material.

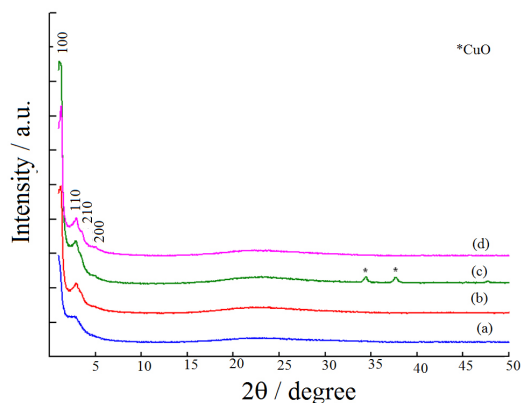


Figure 1. XRD patterns of (a) FeM30; (b) AlM30; (c) CuM30 and (d) pure MCM-41.

The a_0 lattice parameters of the samples, together with their metal loading after the calcination, as measured by AAS, are presented in Table 1.

As can be seen, the iron content is quite similar for both FeM15 and FeM30 (approximately 4.2 wt.%) in spite of the markedly different initial Fe/Si ratio. It could be suggested that a limit concentration for iron incorporation in MCM-41

Table 1. Chemical composition and structural characterization of the samples by XRD, AAS and N_2 sorption analysis

Sample	Composition / wt.%			$d_{100} / \text{Å}$	$a_0 / \text{Å}$	Surface area / ($\text{m}^2 \text{g}^{-1}$)	Pore diameter / Å
	Cu	Al	Fe				
MCM-41	–	–	–	42.6	49.2	1145	42
FeM30	–	–	4.1	48.9	56.5	1009	41
FeM15	–	–	4.3	44.9	51.8	880	42
AlM30	–	3.4	–	44.0	50.8	580	38
AlM15	–	3.5	–	47.3	54.6	848	42
FeAlM30	–	2.3	1.6	41.3	47.7	893	44
CuM30	3.0	–	–	41.3	47.7	807	27
CuM15	1.6	–	–	35.1	40.5	876	46

exists (ca. 0.075 mol%), although a more deep study over Fe-MCM-41 samples, with varying Fe content should be carried out to confirm this. The same trend is observed for the Al containing samples: the Al loading could not be increased up to approximately 3.5 wt.% (0.13 mol%). These results would indicate, at least as a first approximation, that both iron and aluminium are being incorporated inside the framework of MCM-41 during the synthesis of the Me-MCM-41 samples. Aluminium would be present as Al^{III} , in tetrahedral coordination, since this species has an ionic radii (0.050 nm) quite similar to the one corresponding to Si (0.041 nm) in the MCM-41 structure. Incorporated iron would be present in its high spin tetrahedral coordination, as Fe^{III} , which ionic radii (0.063 nm) is quite similar to Si one. Aluminium molar loading is higher than the one corresponding to Fe due to the fact that Al dimension matches better with Si ones. For the same reason, in the case of FeAlM30, the Al molar concentration (0.08 mol%) is higher than the one corresponding to Fe (0.03 mol%).

For both copper containing samples the metal loading is similar to the target one, thus it could be concluded that not all the copper is being introduced inside the framework during the synthesis process and that copper extra-framework species could be also present.

It is worth noting that a_0 parameter of the pure siliceous form is modified by the presence of the metal. This effect has previously been observed for Cu/MCM-41 and Cu/MCM-48.^{24,25} Once again this structural modification could be due to two different phenomena: (i) the insertion of the metal into the silica framework, originating an increase of the wall width and a diminution of the pore diameter, or (ii) the formation of oxide crystals inside the mesopores. Anyway, this a_0 variation is indicative of a high interaction between the metal and MCM-41, whatever be the origin of the interaction.

Besides the analysis of the diffraction peaks at low angles, associated with short range order, interesting results are obtained from the observation of high diffraction angles. Thus, in Figure 1, diffraction peaks associated with bulky Me species appears only for CuM30 sample. These peaks at 37.8° and 43.5° (pattern c) are assigned to CuO. On the other hand, for AlM30 and FeM30, no peaks associated with iron or aluminium bulky species are detected, showing the high dispersion of the corresponding Me species in the MCM-41 structure. In Figure 2, the XRD pattern corresponding to the relatively high loaded samples, FeM15, AlM15, CuM15 and the mixed FeAlM30 are shown. Peaks due to bulky metal species are clearly observed. From these peaks, by the application of the Scherrer approximation, it was calculated that such particles are sized of 24-33 nm for all samples.

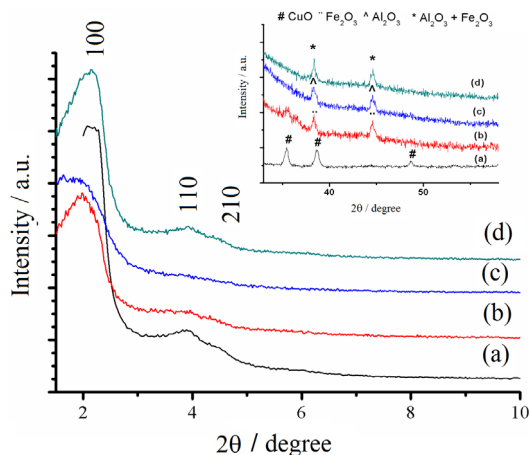


Figure 2. XRD patterns of (a) CuM15, (b) FeM15, (c) AlM15 and (d) FeAlM30 at low angles (inset: XRD at high angles).

To further investigate the nature of the iron, aluminium and copper species in MCM-41, a UV-Visible characterization was carried out. The spectra of the FeM30, FeAlM30 and CuM30 samples before and after calcination, in the 200-700 nm wavelength range are shown in Figure 3. Both as-synthesized samples show a significant absorption in the 200-350 nm range with a maximum at ca. 240 nm, attributable to isolated iron(III) ions in tetrahedral coordination. This band is due to the charge-transfer transition from the oxygen ligand, associated with iron(III) species in tetrahedrally coordinated sites.²⁶ This result confirms that iron species are incorporated in the framework in the as-synthesized samples as iron(III) and are in agreement with the report of Amama *et al.*²⁷

Upon calcination, the spectrum corresponding to FeAlM30 retains the band due to iron(III) in tetrahedral environment, showing that the incorporated iron species are highly stable, and no iron is lodged outside the framework. On the contrary, the band is displaced up to 420 nm for FeM30, which is suggestive of the presence of iron(III) species in octahedral environment, indicating that the calcination treatment dislodges iron into MCM-41 surface, as Fe_2O_3 for the case of this sample. This is not in line with XRD results (no diffraction peaks of iron oxides are detected, see Figure 1). However, it is possible that iron oxide would appear as highly dispersed nanoclusters with particle size lower than the detection limit of the XRD technique.

A UV-Vis analysis was also carried out for CuM30 (Figure 3C). For the sake of comparison, an extra sample of cupric oxide crystals with a size of ca. 30 nm (copper in tetrahedral coordination) supported on SiO_2 (Cu/SiO_2) was also analyzed.²⁸ Both UV-Visible spectra of CuM30 and Cu/SiO_2 are quite similar and it could be concluded that the mesoporous sample only contains bulky copper(II) oxide.

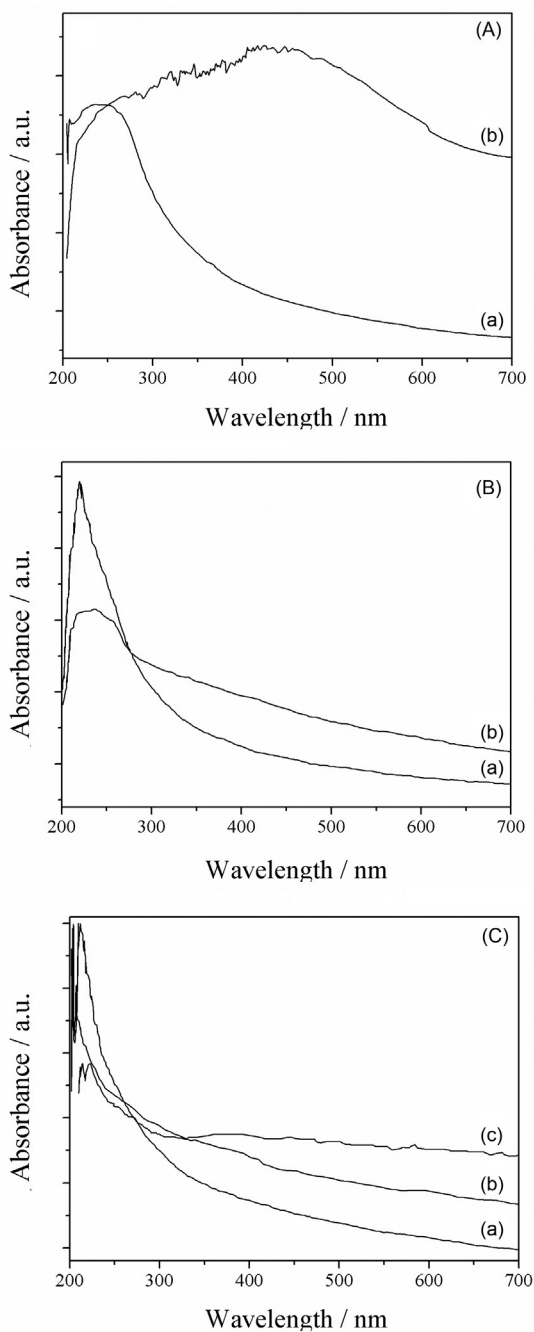


Figure 3. UV-Vis spectra of (A) FeM30: (a) as-synthesized and (b) calcined; (B) FeAlM30: (a) as-synthesized and (b) calcined; (C) CuM30: (a) as-synthesized, (b) calcined and (c) Cu/SiO₂.

The TPR profiles of the samples are presented in Figure 4. As it could be expected, no hydrogen consumption was detected for pure MCM-41, AlM15 and AlM30, since these samples do not present species that undergo reduction in the temperature range of the TPR experiments. On the other hand, the CuM30 sample shows a reduction peak with a maximum at approximately 685 K. A similar behavior was observed for CuM15 sample (data not shown). The quantification of the H₂ consumption indicates that a

complete reduction of CuO to Cu⁰ is accomplished in both samples. In the three iron containing samples, a reduction peak also appears, with a maximum at approximately 670 K. The H₂ consumption shows that the reduction process would be related to the reduction of Fe₂O₃ to Fe₃O₄.

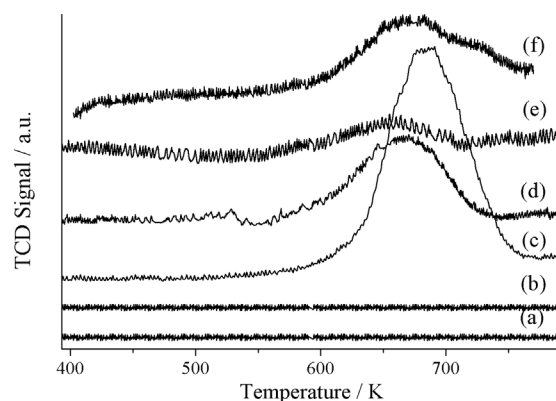


Figure 4. TPR curves: (a) MCM-41; (b) AlM30; (c) CuM30; (d) FeM30; (e) AlFeM30 and (f) FeM15.

Summing up, the TPR results indicate that no redox sites are created due to the incorporation of aluminium. On the other hand, both iron and copper introduce redox properties to MCM-41.

The characteristic morphology of the MCM-41 structure is observed in the HRTEM of the prepared samples. A hexagonal and regular array of uniform channels can be seen in the materials, with each pore surrounded by six neighbors. A more regular hexagonal arrangement of uniform pores at longer range is observed for MCM-41. This mesoporous material presents a decrease in the order of the hexagonal structure with the metal content, as previously concluded from XRD analysis of low diffraction peaks. A representative image of the material AlM30 is shown in Figure 5.

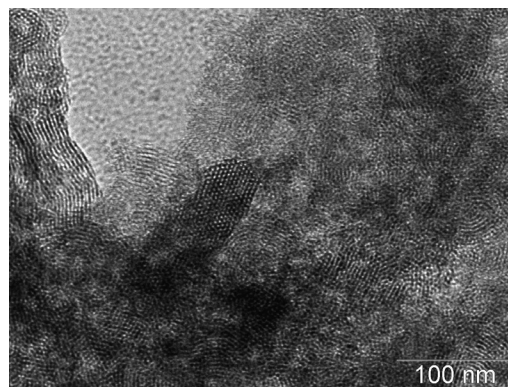


Figure 5. HRTEM of AlM30.

Total surface acidity of mesoporous samples was measured with a potentiometric method by titration with

n-butylamine. Although this method does not allow to distinguish between Lewis or Brønsted acid sites, it gives a general measurement of the acidity of a solid, which is a property of paramount importance for characterizing a solid surface. The potential corresponding to the first point of the titration (E_0 , mV) of the non-aqueous suspension allows the solid to be classified according to its acid strength.²² The following scale has been assumed: $E_0 > 100$ mV (very strong sites), $0 < E_0 < 100$ mV (strong sites), $-100 < E_0 < 0$ mV (weak sites) and $E_0 < -100$ mV (very weak sites). The total number of acid sites can be estimated from the amount of base added to reach the constant potential value in the titration curve. The values of acid strength, total acidity, and density of acid sites for the prepared samples are presented in Table 2. The results indicate that while the MCM-41 material exhibits weak acid sites with an E_0 value of -13.8 mV, the AIM30 sample exhibits the highest value (27.2 mV). According to Choundhary and Mantri,²⁹ surface acidity in non-substituted MCM-41 materials is due to two types of terminal silanol groups (isolated and differently bonded to hydrogen silanol groups). From these results, it can be concluded that the acid strength increases with the aluminium content.

Table 2. Determination of total acidity through titration with *n*-butylamine

Sample	E_0 / mV	Total acid strength	Total number of acid sites / (mmol g ⁻¹)	Density of acid sites / (μmol m ⁻²)
MCM-41	-13.8	w ^a	2.08	1.82
AIM30	27.2	s ^b	1.21	2.09
FeAIM30	-29.8	w	0.69	0.77
FeM30	-30	w	1.56	1.55
CuM30	-27	w	1.73	2.14

^aw: weak; ^bs: strong.

In spite of the similar Al content in AIM30 and FeAIM30 (see Table 1), the latter sample shows lower acidity and acid strength than the former, and this fact could be attributed to a partial obstruction of the acid sites generated by the deposition of Fe₂O₃ on the surface of the support after the calcination process.

In order to further analyze with more detail the acidic nature of the different samples, an FTIR study of adsorbed pyridine was carried out. This technique allows to distinguish between Lewis and Brønsted acidity and also to determine the concentration of the sites from the quantification of the corresponding bands. In Figure 6, the spectra corresponding to pyridine adsorbed on FeM30, AIM30 and AlFeM30 are shown. Pyridine adsorption yields IR bands characteristic of pyridinium ion (PyH⁺) with

vibration at around 1624 cm⁻¹. In addition, a band resulting from coordinatively bonded pyridine on electron acceptor sites (Lewis centers) was observed at ca. 1460 cm⁻¹. It can be concluded that FeM30, AIM30 and AlFeM30 possess both Lewis and Brønsted acidity. On the other hand, for the adsorption of pyridine onto CuM30 and MCM-41 (data not shown), the results indicated that no Brønsted acidity is present in these samples. This is a quite interesting fact that can be related with the above proposed description of Me-MCM-41. We have postulated that while Fe and Al are incorporated in the siliceous network, Cu remains as extra-framework species. Thus, it could be concluded that intra-framework Fe and Al species give rise to Lewis acid centers, which originates the already mentioned bands ca. 1460 cm⁻¹. In addition, the band at 1490 cm⁻¹ suggests the formation of the adjacent Lewis and Brønsted acid sites.³⁰ The concentration of Lewis sites was calculated according to equation $\epsilon(L) = A_L/10c_L$, where $\epsilon(L)$ is the extinction coefficient of the Lewis species ($\epsilon(L) = 2.22 \pm 0.1$ cm μmol⁻¹), A_L is the area of the characteristic band at 1455 cm⁻¹ (mg⁻¹ cm² cm⁻¹) for a sample of thickness 10 mg cm⁻², and c_L is the molar concentration of Lewis sites (mmol g⁻¹).²³ The corresponding data are summarized in Table 3. As can be observed, the major Al content increases the Lewis acidity of the MCM-41.

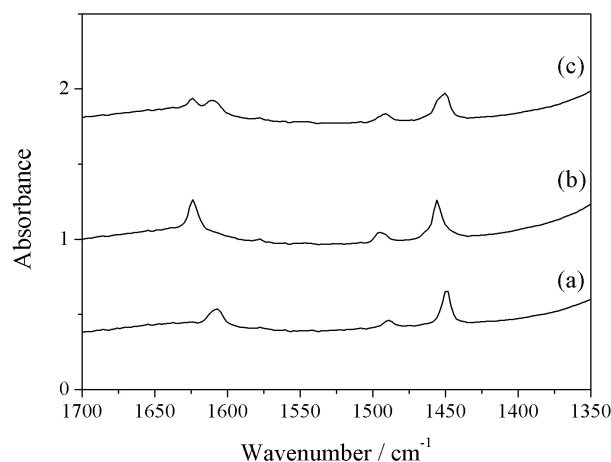


Figure 6. FTIR spectra of 3 Torr of pyridine adsorbed over (a) FeM30; (b) AIM30 and (c) FeAIM30.

Table 3. Concentration of Lewis sites calculated according to equation $\epsilon(L) = A_L/10c_L$

Desorption temperature / K	AIM30 C_{Lc} / (mmol g ⁻¹)	FeM30 C_{Lc} / (mmol g ⁻¹)	FeAIM30 C_{Lc} / (mmol g ⁻¹)
423	0.117	0.090	0.096
523	0.069	0.048	0.062

From the study of the acidic properties of the samples, both from titration with *n*-butylamine and FTIR of

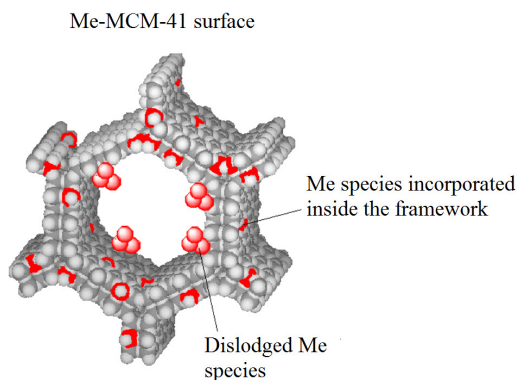
Table 4. Variation of cell parameters after the hydrothermal studies

Temperature / K	$a_0 / \text{Å}$					
	AlM30			FeM30		
	pH 3	pH 6	pH 10	pH 3	pH 6	pH 10
303	53.7	51.9	54.6	50.21	51.52	52.59
333	51.9	53.7	56.5	50.21	51.73	–
363	51.1	53.7	–	50.21	50.26	–

^a a_0 in as-synthesized samples after calcinations.

adsorbed pyridine, one can conclude that the introduction of aluminium species into MCM-41 is a way to noticeably increase the acidity of the mesoporous system.

Finally, based on the whole of the characterization results, a model for Me-MCM-41 has been built (Figure 7). Two different metal species are envisaged, one of them corresponds to metal buried in the framework, while the other one constitutes extra-framework bulky oxide. For both Al-MCM 41 samples (AlM30 and AlM15) the former species would be the predominant one, while for all mesoporous samples containing Fe and Cu both species would coexist. The fraction of extra-framework species is higher for Cu-MCM-41 than for Fe-MCM-41. The model is in line with the decreasing ionic radii in the following order: $\text{Al}^{\text{III}} < \text{Fe}^{\text{III}} < \text{Cu}^{\text{II}}$. Extra-framework Me species show the corresponding diffraction peaks in XRD and for the case of copper and iron, are engaged in redox changes, as measured by TPR. Me species inside the MCM network originate a distortion in the order of the mesoporous systems, and are related to the Lewis acidity of the samples, mainly in the case of aluminum.

**Figure 7.** Schematic description of the two possibilities of Me interaction with MCM-41.

Stability of Me-MCM-41 in water

The stabilities of AlM30 and FeM30 were investigated by measuring the decrease in intensity of low diffraction

XRD peaks of MCM-41 at different temperatures and pH values. As it will be seen later, these two samples present higher adsorption properties than the other ones. This is the reason why AlM30 and FeM30 were selected for studying the stability in aqueous media.

The AlM30 and FeM30 structures are stable for 8 h in water between pH 3-6 as concluded from the fact that the MCM-41 mesoporous structure is kept over the entire range of temperatures studied. At pH 10 and a 303 K, the solid suffers a partial disintegration, which is completed at higher temperatures. This is an expected result due to the hard alkaline conditions.³¹ This fact is summarized in the Table 4.

Phenol adsorption

In order to study the effect of the different metals Cu, Fe and Al in MCM-41 on the adsorption of PhOH, adsorption experiments were conducted using the samples with Si/Me ratio = 30 and also over activated carbon and over SiO_2 ($210 \text{ m}^2 \text{ g}^{-1}$) for the sake of comparison. The results of the adsorption experiments, expressed as g of PhOH adsorbed *per* 100 g of adsorbent and as mol of PhOH adsorbed *per* m² of exposed area of the adsorbent are shown in Table 5.

Table 5. Adsorption of phenol on Me-modified mesoporous materials at pH 6 and 303 K

Adsorbent	Phenol adsorbed / wt. %	Specific phenol adsorbed / mol of the phenol adsorbed <i>per</i> m ² of the adsorbent
Activated Carbon	38.6	nd ^a
SiO_2	0	0
MCM-41	19.5	1.8×10^{-6}
FeM30	16.0	1.7×10^{-6}
FeAlM30	16.4	2.0×10^{-6}
CuM30	12.4	1.6×10^{-6}
AlM30	24.9	4.6×10^{-6}
AlM30 ^b	54.2	1.0×10^{-5}

^and: not determined; ^bpH 3.

Silica is completely inert towards phenol; on the contrary all the other samples retain certain amount of the pollutant. Since the pure siliceous form, MCM-41 does not possess redox or acid-base properties (at least in comparison to the other mesoporous samples) that could interact with phenol, it could be concluded that the retention properties of MCM-41 are originated by the tortuosity of its structure, and mainly physical interaction would be developed between phenol and MCM-41. The tortuosity of MCM-41 is not modified upon the introduction of Al, Fe or Cu since these species slightly modify the pore diameter sizes, and the curvature of the channels (the main property of a porous solid related to tortuosity) is not altered.

The introduction of copper to MCM-41 (CuM30 sample) does not increase adsorption properties, showing that copper redox sites are not reactive towards phenol. In the same sense, iron species (also associated with surface redox sites) should not be considered as a promoter for phenol retention. As a general trend, it is concluded that redox sites do not increase the desired properties of MCM-41 and that over this latter material, as well as in the case of Cu-MCM-41 and Fe-MCM-41 the adsorption of phenol is due to physical interaction between the solid surface and phenol related with the tortuosity of these materials. Concomitantly, these samples show quite similar values for the specific phenol retention (see Table 5). This conclusion stands for both cases: when the retention capacity is expressed *per* mass of adsorbent and when it is reported *per* specific surface area.

Although the highest capacity of adsorption corresponds to activated carbon, AIM30 possess a relatively high capacity of retention. Even more, this capacity is increased if the adsorption process is carried out in an acidic media (Table 5). Following characterization of by adsorbed pyridine-FTIR and of titration with *n*-butylamine, it was concluded that AIM30 shows the major surface acidity properties. This acidic nature would be the origin of the relatively high capacity of AIM30 for retaining phenol. Since no other mesoporous sample showed an acidity of the same magnitude as AIM30, it can be concluded that acidic sites are the main responsible for phenol adsorption in AIM30.

For AIM30, the adsorption of PhOH is significantly affected by pH: at pH > 10 the adsorption capacity decreases not only for the partial destruction of the mesoporous structure due to the alkaline media, in line with the above commented stability study, but also for the phenol-phenolate equilibrium shift (pKa phenol ca. 10). The opposite effect is observed at acidic pH, for which the adsorption capacity is increased, probably due to electrostatic interactions between hydroxyl groups of

phenol and silanol groups and/or to the Lewis acid-base affinity of π -electrons of aromatic ring with the acidic sites in the Al incorporated MCM-41.¹³

The increased absorption of phenol over AIM30 under acidic conditions is in line with the results of the FTIR study over sample AIM30 at room temperature (Figure 8). The fresh sample before phenol adsorption (Figure 8a) shows a typical band attributable to Si–O–Al vibrations at 950 cm^{-1} .

Besides, a sharp band at ca. 3700 cm^{-1} is observed, which is ascribed to free Si–OH groups, single and/or germinal.^{16,32,33} This band shows a shoulder at low frequency side which is due to the interaction of silanol groups with adsorbed water molecules. Upon phenol adsorption, the intensity of the former shoulder notably increases due to interaction of adsorbed phenol and water with the free silanol groups. Such an increase was detected for all the Me-MCM-41 samples. An additional band at 1480 cm^{-1} was detected in the spectrum of AIM30 before contacting with phenol, and it was not observed for the other samples. The fact that this band is not detected for the other samples submitted to phenol contact indicates that it is associated with the higher capacity of AIM30 for retaining phenol. So it can be concluded that the phenol adsorption proceeds via π -electrons of the aromatic ring with the acidic sites of the AIM30 material.

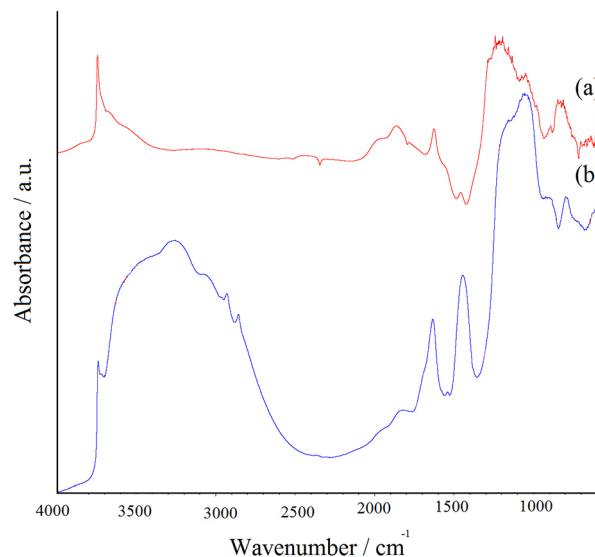


Figure 8. FTIR spectra of AIM30 before (a) and after phenol adsorption (b).

Conclusions

The introduction of Al, Cu or Fe in MCM-41 decreases the short range order of the solid network and modifies the physicochemical properties of the mesoporous solid, as it is evident from the XRD, TEM, TPR, *n*-butylamine titration and FTIR of adsorbed pyridine results.

Aluminium is mainly incorporated in the mesoporous walls of MCM-41, while iron and copper are distributed as incorporated and extra-framework species.

All the mesoporous samples are stable in acidic and neutral pH, even at temperatures up to 363 K. In alkaline media, the structure suffers a partial disintegration and this effect is more notorious at high temperatures.

The presence of Al in the framework of MCM-41 increases phenol adsorption which is heavily dependent on the pH of the solution, and would be related to the creation of new acidic sites on the siliceous material.

Al-MCM-41 could be envisaged as a material for eliminating phenol from water, mainly due to its relative high capacity of retention and its stability properties under reaction conditions.

Acknowledgements

This work was supported by grants from the Consejo Nacional de Investigaciones Científicas y Técnicas (CONICET) and Universidad Nacional del Sur (UNS). The authors would like to thank PhD Daniel Vega (CNEA, Comisión Nacional de Energía Atómica, Centro Atómico Constituyentes, Buenos Aires, Argentina) for some XRD measurements and PhD Sergio Moreno (CNEA, Comisión Nacional de Energía Atómica, Centro Atómico Bariloche, Río Negro, Argentina) for the HRTEM determinations and to PhD M. Dennehy and PhD D. Vitvarová for FITR measurements.

References

1. Neimark, A. V.; Ravikovitch, P. I.; Grun, M.; Schuth, F.; Unger, K. K.; *J. Colloid Interf. Sci.* **1998**, *207*, 159.
2. Feng, X.; Fryxell, G. E.; Wang, L. Q.; Kim, A. Y.; Liu, J.; Kemner, K. M.; *Science* **1997**, *276*, 923.
3. Liu, J.; Feng, X.; Fryxell, G. E.; Wang, L. Q.; Kim, A. Y.; Gong, M.; *Adv. Mater.* **1998**, *10*, 161.
4. Sayari, A.; Hamoudi, S.; Yang, Y.; *Chem. Mater.* **2005**, *17*, 212.
5. Lam, K. F.; Chen, X.; McKay, G.; Yeung, K. L.; *Ind. Eng. Chem. Res.* **2008**, *47*, 9376.
6. Fryxell, G. E.; Liu, J.; Hauser, T. A.; Nie, Z.; Ferris, K. F.; Mattigod, S.; Gong, M.; Allen, R. T.; *Chem. Mater.* **1999**, *11*, 2148.
7. Samadi-Maybodi, A.; Teymouri, M.; Vahid, A.; Miranbeigi, A.; *J. Hazard. Mater.* **2011**, *192*, 1667.
8. Horcajada, P.; Rámila, A.; Férey, G.; Vallet-Regí, M.; *Solid State Sci.* **2006**, *8*, 1243.
9. Zhao, X. S.; Lu, G. Q.; *J. Phys. Chem. B* **1998**, *102*, 1556.
10. Zhou, Y.; Tao, Y. F.; Yang, J.; Lin, W. G.; Wan, M. M.; Wang, Y.; Zhu, J. H.; *J. Hazard. Mater.* **2011**, *190*, 87.
11. Fu, J.; He, Q.; Wang, R.; Liu, B.; Hu, B.; *Colloids Surf., A* **2011**, *375*, 136.
12. Mangrulkar, P. A.; Kamble, S. P.; Meshram, J.; Rayalu, S. S.; *J. Hazard. Mater.* **2008**, *160*, 414.
13. Kim, Y.; Lee, B.; Choo, K.; Choi, S.; *Micropor. Mesopor. Mater.* **2011**, *138*, 184.
14. Huang, L.; Huang, Q.; Xiao, H.; Eić, M.; *Micropor. Mesopor. Mater.* **2007**, *98*, 330.
15. Ahmaruzzaman, M.; *Adv. Colloid Interface Sci.* **2008**, *143*, 48.
16. Huang, L.; Xiao, H.; Ni, Y.; *Colloids Surf., A* **2004**, *247*, 129.
17. Luchian, C.; Niculaua, M.; Cotea, V. V.; Bilba, N.; Copcia, V.; Sandu, A. V.; *Rev. Chim. (Bucharest, Rom.)* **2011**, *62*, 287.
18. Zhao, X. S.; Lu, G. Q.; Millar, G. J.; *Ind. Eng. Chem. Res.* **1996**, *35*, 2075.
19. Corma, A.; *Chem. Rev.* **1997**, *97*, 2373.
20. Selvam, P.; Bhatia, S. K.; Sonwane, C. G.; *Ind. Eng. Chem. Res.* **2001**, *40*, 3237.
21. Bore, M. T.; Mokhonoana, M. P.; Ward, T. L.; Coville, N. J.; Datye, A. K.; *Micropor. Mesopor. Mater.* **2006**, *95*, 118.
22. Cid, R.; Pecchi, G.; *Appl. Catal., A* **1985**, *14*, 15.
23. Wichterlová, B.; Tvarůžková, Z.; Sobalík, Z.; Sarv, P.; *Micropor. Mesopor. Mater.* **1998**, *24*, 223.
24. Gutiérrez, V. S.; Diez, A. S.; Dennehy, M.; Volpe, M. A.; *Micropor. Mesopor. Mater.* **2011**, *141*, 207.
25. Gomes, H. T.; Selvam, P.; Dapurkar, S. E.; Figueiredo, J. L.; Faria, J. L.; *Micropor. Mesopor. Mater.* **1998**, *24*, 223.
26. Li, B.; Wu, K.; Yuan, T.; Han, C.; Xu, J.; Pang, X.; *Micropor. Mesopor. Mater.* **2012**, *151*, 277.
27. Amama, P. B.; Lim, S.; Ciuparu, D.; Yang, Y.; Pfefferle, L.; Haller, G. L.; *J. Phys. Chem. B* **2005**, *109*, 2645.
28. Gutiérrez, V. S.; Dennehy, M.; Diez, A. S.; Volpe, M. A.; *Appl. Catal., A* **2012**, *437*, 72.
29. Choundary, V. R.; Mantri, K.; *Micropor. Mesopor. Mater.* **2000**, *40*, 127.
30. Khder, A. E. R. S.; Hassan, H. M. A.; Shall, M. S. E.; *Appl. Catal., A* **2012**, *411*, 77.
31. Chen, L. Y.; Jaenicke, S.; Chuah, G. K.; *Microporous Mater.* **1997**, *12*, 323.
32. Chen, J.; Li, Q.; Xu, R.; Xiao, F.; *Angew. Chem., Int. Ed. Engl.* **1995**, *34*, 2694.
33. Jentys, A.; Pham, N. H.; Vinek, H. J.; *J. Chem. Soc., Faraday Trans.* **1996**, *92*, 3287.

Submitted: March 3, 2015

Published online: May 15, 2015